Self-Assembling Protein Hydrogels with Modular Integrin Binding Domains

Lixin Mi, Stephen Fischer, Brian Chung, Sarah Sundelacruz, and James L. Harden*

Department of Chemical & Biomolecular Engineering, Johns Hopkins University, Baltimore, Maryland 21218

Received March 3, 2005; Revised Manuscript Received October 24, 2005

Hydrogels with integrin binding activity were created from associating proteins with embedded RGD sequences. These proteins are a modified AC_{10}Bcys triblock design composed of acidic A and basic B leucine zipper associating domains flanking a new soluble disordered coil block that contains nine repeats of AGAGAGPEG and three copies of the RGD integrin binding sequence. As with the original AC_{10}Bcys design without the embedded RGD sequences, these proteins self-assemble into stable hydrogels at concentrations above approximately 50 mg/mL in a range of solution pH and temperature conditions. The mechanism for hydrogel assembly is the intermolecular association of A and B helical domains into bundles which act as cross-links connected by the soluble central disordered coil domains. The secondary structure of the proteins and the mechanical properties of the hydrogels they form are not adversely affected by the presence of the RGD sequences. The RGD sequences embedded in the disordered coil region support the adhesion, spreading, and polarization of human fibroblast cells on protein coated surfaces. Confocal microscopy studies demonstrated the presence of focal adhesion complexes and organized actin stress fibers in these cells. In contrast, fibroblasts seeded onto surfaces coated with the original AC_{10}Bcys protein remained rounded and did not form focal adhesions, indicating that bioactivity is conferred by the presence of the embedded RGD sequences. Such hydrogel-forming bioactive proteins have potential for cell and tissue culture applications.

Introduction

The design of materials with tailored biofunctional attributes has been a major focus of the biomaterials community in recent years.[1,2] In such materials, established mechanisms of biological recognition have been incorporated to provide specific biochemical signals to their intended biological environment. For the case of materials for cell and tissue engineering, for instance, elements that mimic particular cell adhesion or signaling ligands in the extracellular matrix (ECM) have been utilized in many systems. In particular, as an alternative to biomaterials comprised of native ECM proteins such as fibronectin, vitronectin, and collagen, minimalist oligopeptide sequences that mimic their functions[3,4] have been successfully employed in a variety of biomimetic materials designs.

Perhaps the most extensively studied ligands are those that selectively bind the integrin receptors displayed on many mammalian cell types.[5] The integrin-binding activity of natural adhesion proteins can be partially reproduced by short oligopeptide sequences, such as the ubiquitous RGD tripeptide sequence.[4] Although using short peptide sequences may lead to a reduction in overall biological activity, they have several inherent advantages. As short peptide sequences, they are usually more stable than native adhesion proteins and allow for enhanced control over ligand presentation. Most importantly, they encode a very specific biological signal and thereby eliminate the possibility of additional undesired cellular signals.

Integrin-binding ligands have been utilized in a variety of biomaterials platforms, including synthetic and natural polymer hydrogels,[6−10] surface-functionalized polymers,[11,12] hybrid peptide amphiphiles,[13] and genetically engineered silk-based[14,15] and elastin-based[16−20] biomaterials. In all of these cases, the integrin-binding ligand was crucial for eliciting cell attachment and phenotypical response to the biomaterial. For example, synthetic poly(ethylene glycol) hydrogels photochemically functionalized with RGD peptides have been shown in early work to promote attachment and spreading of fibroblasts.[6] Hydrogels are particularly attractive biomaterials for tissue engineering due to their ability to retain water and soluble proteins such as growth factors within the gel network, and to maintain chemical and osmotic equilibria with the surrounding media. Moreover, their viscoelastic properties and structural stability can be controlled by design, enhancing their utility as structural scaffolds for cell culture.

As an alternative to synthetic polymer hydrogels, we are interested in the use of genetically engineered protein hydrogels for tissue engineering applications. Protein-based hydrogels are potentially biocompatible and are biodegradable by the normal protein turnover pathways. Moreover, these hydrogels can also be designed to reversibly self-assemble from a solution of associating proteins in response to a change in pH or temperature. A great advantage of utilizing proteins as the macromolecular constituents of a hydrogel is the ability to construct modular polymer-like proteins composed of several functionally independent domains. In particular, the structural and bioactive features of such proteins can be separately engineered to achieve specific biomimetic attributes. Using standard molecular biology tools, one may dictate the precise sequence of a de novo protein design and faithfully produce this protein in large quantities in a host organism such as *E. coli*.

In this study, a hydrogel-forming triblock protein with embedded integrin-binding RGD sequences is presented and characterized. This triblock protein is based on an established de novo protein design, AC_{10}Bcys, consisting of a central soluble

* To whom correspondence should be addressed at Dept. of Physics, University of Ottawa, Ottawa, Ontario K1N 6N5, Canada. E-mail: jharden@science.uottawa.ca.

10.1021/bm050157p CCC: $33.50
Published on Web 12/13/2005

WPT2 ($AC_{10}B_{cys}$)
230 residues; 22447 Daltons
MRGSHHHHHHGSDDDDKWASGDLENEVAQLEREVRSLEDEAAELEQKVSRLK
NEIEDLKAEIGDHVAPRDTSYRDPMGAGAGAGPEGAGAGAGPEGAGAGAGPEG
AGAGAGPEGAGAGAGPEGAGAGAGPEGAGAGAGPEGAGAGAGPEGAGAGAGP
EGAGAGAGPEGARMPTSGDLKNKVAQLKRKVRSLKDKAAELKQEVSRLENEIE
DLKAKIGDHVAPRDTSMGGC
WPT2-3R
251 residues; 24597 Daltons
MRGSHHHHHHGSDDDDKWASGDLENEVAQLEREVRSLEDEAAELEQKVSRLK
NEIEDLKAEIGDHVAPRDRGTPPGAGAGAGPEGAGAGAGPEGAGAGAGPEGAV
RPMASVD**RGD**SGAGAGAGPEG**RGD**SGSELAGAGAGPEG**RGD**SGAGAGAGPEG
GSARQGAGAGAGPEGAGAGAGPEGAGAGAGPEGRMPTSGDLKNKVAQLKRKV
RSLKDKAAELKQEVSRLENEIEDLKAKIGDHVAPRDTSMGGC

Figure 1. The helical regions are underlined and the RGD motifs are highlighted in bold font.

disordered coil domain flanked by associating leucine zipper end domains.[21−23] The gene encoding the original repetitive C_{10} = $(AGAGAGPEG)_{10}$ center domain has been reconstructed to remove repetition in the oligonucleotide sequence. The new disordered coil gene fragment is composed of a nonrepetitive DNA sequence that encodes nine repeats of AGAGAGPEG with three distributed repeats of the RGD sequence. The terminal A and B leucine zipper domains of WPT2 are retained in our protein. The biofunctional triblock protein incorporating this new center domain is denoted WPT2−3R. The details of the synthesis of WPT2−3R and the degenerate codon scrambling method used for reconstructing the center block are presented in a separate paper.[24] This paper focuses on the molecular characterization of WPT2−3R, the materials properties of the hydrogels that self-assemble from it, and the response of human foreskin fibroblast (HFF) cell lines to surfaces coated by these hydrogel materials.

Materials and Methods

Protein Synthesis and Purification. Standard molecular biology methods were used for preparation and manipulation of DNA oligonucleotides, artificial gene assembly, cloning, bacterial growth, and protein expression and purification.[25,26] A detailed description of these procedures for WPT2−3R is given elsewhere.[24,27] Here we provide a brief summary. Synthetic oligonucleotides were purchased from MWG Biotech Inc. (High Point, NC). All enzymes and associated reagents were purchased from New England Biolabs (Beverly, MA). The pUC-19 cloning vector and the Platinum *Pfx* DNA Polymerase were purchased from Invitrogen Inc. (Carlsbad, CA). The XL-1 Blue cloning *E. coli* strain and dNTP were purchased from Stratagene Inc. (La Jolla, CA). The SG13009 expression *E. coli* strain, DNA purification kits, and Ni−NTA resin were purchased from Qiagen (Valencia, CA). Isopropyl-1-β-D-thiogalactoside (IPTG) was purchased from Calbiochem (San Diego, CA). All other chemicals were purchased from Sigma-Aldrich (St. Louis, MO).

The expression plasmid pQE9-L2AC_{10}B encoding the original triblock protein AC_{10}Bcys (which we will designate as WPT2) was kindly provided by the group of David Tirrell at the California Institute of Technology. WPT2 is composed of a disordered coil domain (C_{10}) flanked by an acidic (A) and a basic (B) leucine zipper domain. WPT2 also includes a hexahistidine tag and an enzymatic cleavage site at the N-terminus and a cysteine residue at the C-terminus. The amino acid sequence for WPT2 is given in Figure 1. DNA encoding the modified center block was prepared by polymerase chain reaction methods using a Genius thermocycler (Techne Inc., Burlington, NJ) and ligated into the pUC-19 cloning vector as a replacement for the C_{10} section of the WPT2 gene.[24,27] XL-1 Blue competent cells were transformed by the resulting circular plasmid pUC-19-WPT2−3R using the heat shock method. Transformants were cultured on LB agar plates under ampicillin selection (100 μg/mL) at 37 °C for 16 h. Positive transformants were selected by the colony-PCR screening technique and used to inoculate 5 mL of LB medium with ampicillin (100 μg/mL). Plasmid DNA was isolated by a Qiaprep plasmid miniprep kit and sequenced at the Johns Hopkins University Core Facility to verify sequence correctness of the gene of interest, which encodes WPT2−3R. The amino acid sequence for WPT2−3R is given in Figure 1. Note that WPT2−3R retains the A and B leucine zipper domains of WPT2, as well as its N-terminal hexahistidine tag and C-terminal cysteine residue. Following sequence verification, the WPT2−3R gene was ligated into the pQE−9 expression vector, and the expression plasmid pQE−9-WPT2−3R was transformed into the *E. coli* expression host SG13009 (containing the *trans*-regulator-pREP4 plasmid) using the heat-shock method. Transformed cells were spread onto agar plates with both ampicillin (100 μg/mL) and kanamycin (25 μg/mL) and incubated for 16 h at 37 °C. A positive transformant was selected and used to inoculate 10 mL of LB medium with both ampicillin (100 μg/mL) and kanamycin (25 μg/mL). The culture was incubated in a shaker-incubator at 37 °C and 300 rpm until achieving an optical density at 600 nm (OD_{600}) of 0.6. The cells in 2 mL of culture were harvested to produce glycerol-stock, which was stored at −80 °C for future seedings.

Large scale protein expression was carried out in a 5 L Biostat B fermentor (Sartorius BBI Systems Inc., Allentown, PA) as follows. Ten microliters of glycerol stock was used to inoculate 10 mL of LB medium. The medium was shaken at 37 °C and 300 rpm for 5−7 hours until the OD_{600} reached 0.6. Four milliliters of this medium was used to prepare a 200 mL overnight culture, which was shaken at 30 °C and 300 rpm for 12−16 h. This overnight culture was employed for high cell density fermentation at the inoculums to fresh medium volume ratio of 1:50 using an enriched LB medium containing 3.5 g of KH_2PO_4, 5.0 g of K_2HPO_4, 3.5 g of $(NH_4)_2HPO_4$, 0.5 g of $MgSO_4 \cdot 7H_2O$, 30 g of glucose, 10 g of casein, 5 g of yeast extract, and 5 g of NaCl per liter of medium. Batch-mode fermentation was conducted at 37 °C and pH 6.9 in the presence of oxygen, antibiotics, and anti-foaming agents. The culture was induced at an OD_{600} near 28 by the addition of IPTG, and protein expression was halted when the OD_{600} reached 40 in approximately 4 h. The cells were harvested by centrifugation at 3000*g* for 30 min at 4 °C, typically yielding a wet cell mass of about 40−50 g per liter of culture media.

Harvested cells were resuspended in 6 M GuHCl and frozen at −80 °C. The frozen cell suspension was thawed and sonicated for 30 min to disrupt the cells. The resulting cell lysate was centrifuged at 10 000*g* for 30 min at 4 °C. Purification of the His-tagged proteins was

performed using a modified FPLC (Amersham Pharmacia) with Ni−NTA agarose resin from Qiagen. The collected centrifuge supernatant was first filtered through a 0.45 μm membrane before being loaded onto a Ni−NTA agarose resin column preequilibrated with 5 column volumes of buffer B (8 M urea, 100 mM sodium phosphate, and 10 mM Tris, pH 8.0). The column was sequentially washed with 6 volumes of buffer B and 6 volumes of buffer C (8 M urea, 100 mM sodium phosphate, and 10 mM Tris, pH 6.3). Finally, the His-tagged WPT2−3R was eluted by a continuous stream of buffer E (8 M urea, 100 mM sodium phosphate, and 10 mM Tris, pH 4.5). The contents of all wash and elution fractions were checked by sodium dodecyl sulfate-polyacrylamide gel electrophoresis (SDS−PAGE). The target-protein elution was concentrated 10−30-fold using a VivaFlow 50 ultrafiltration unit (Viva Science Inc., Hannover, Germany). The concentrated protein solution was loaded into dialysis tubing (10 kDa MWCO, Spectrum Labs), dialyzed against continuously replenished reverse-osmosis purified water, and subsequently freeze-dried. Further purification was conducted by reverse-phase high performance liquid chromatography (HPLC) on a Waters 510 HPLC with a C4 analytical column using the gradient elution method. Reverse-phase HPLC, SDS−PAGE, and matrix-assisted laser desorption ionization-time-of-flight mass spectroscopy (MALDI-TOF) were used to characterize protein molecular weight and purity. Amino acid composition analysis was performed by the Keck Biotechnology Resource Laboratory at Yale University. MALDI-TOF mass spectroscopy was conducted on a Voyager DE-STR (Applied Biosystems) at the Johns Hopkins University Mass Spectrometry and Proteomic Facility using standard procedures.

Circular Dichroism. Circular dichroism (CD) spectroscopy was carried out on an Aviv 215 spectropolarimeter (Lakewood, NJ) in the presence of continuous nitrogen flushing. Quartz cuvettes with path lengths of 10 mm were used as sample cells. Measurements were conducted with a resolution of 0.1 nm, a bandwidth of 0.5 nm, a scan speed of 10 nm/s, and a sensitivity of 100 mdeg. The scan range was from 200 to 250 nm. An average of three scans was reported for each set of measurement conditions. All of the samples were prepared from stock solutions (approximately 5 mg of protein per mL) in 10 mM sodium borate phosphate buffer (pH 7.0). The concentrations of protein stock solutions were determined by absorbance at 280 nm in ultrapure grade 6 M guanidine hydrochloride (extinction coefficient, $\epsilon = 5690$ cm^{-1} M^{-1}, 1 tryptophan per protein) by a Cary 50 UV/vis spectrophotometer (Varian Inc.) using standard protocols. CD wavelength scans were conducted on 2.5 μM solutions in 10 mM sodium borate phosphate buffer at three pH levels (6.5, 7.5, and 8.5). The results were expressed as mean residue molar ellipticity [Θ] with units of deg cm^2 $dmol^{-1}$ res^{-1} as calculated using $[\Theta] = \Theta_{obs}/(10cln)$, where Θ_{obs} is the observed ellipticity in mdeg, c is the protein concentration in molar units, l is the path length in cm, and n is the number of amino acid residues in the protein. The fractional helical content f was estimated by the ratio of the observed value of [Θ] at $\lambda = 222$ nm to the value for a purely helical sequence of n amino acids as determined from a representative set of proteins with known secondary structure:[28] $f = [\Theta]_{222}/[\Theta^{helix}]_{222}$, where $[\Theta^{helix}]_{222} = -39\,500(1 - 2.57/n)$.

Diffusing Wave Spectroscopy. Diffusing wave spectroscopy (DWS), dynamic light scattering in the highly multiple-scattering limit,[29] was used as an optical probe of the viscoelasticity of the protein hydrogels. The temporal intensity autocorrelation function of light multiply scattered by a dilute suspension (0.5% solids diluted from stock) of 1 μm diameter sulfonated polystyrene tracer particles (Interfacial Dynamics Corporation) embedded in various hydrogel samples was measured and used to monitor the thermally induced fluctuations of the tracer particles as follows. DWS samples with 7.5% (w/v) protein and 0.5% (w/v) tracer particles were prepared by mixing purified dry protein with 100 mM sodium borate phosphate buffer at pH 6.5 in a clean glass cuvette maintained at 75 °C. After the protein was fully dissolved, a stock tracer particle solution was added to the gel to achieve a final particle concentration of 0.5% (w/v). The gel containing the tracer particles was allowed to equilibrate for approximately 12 h prior to DWS measurements. Sample pH was adjusted between pH 6.5 and pH 9.0 by the addition of 10M NaOH stock. Hydrogel samples contained in a 5 mm path length optical cuvette (Starna cell Inc) were maintained a temperature between 25 and 65 °C by temperature-controlled oil bath and illuminated with a coherent laser source (LightWave Inc) operating at 512 nm and 400 mW. In the transmission geometry, the forward scattered light was split and simultaneously directed to two detector systems, a photomultiplier (PMT) system and a CCD-based system.[30,31] For the case of the PMT detector system, light scattered by the sample was first re-scattered by a second reference cell, a roughened glass frit translated sinusoidally by a driven piezoelectric stage, and then captured by a single-mode optical fiber and directed to a pair of Hamamatsu PMTs. The amplified signal from the two PMTs was then cross-correlated by a multi-tau digital correlator (correlator.com) to obtain a time-averaged intensity autocorrelation function for the composite two-cell system. The corresponding autocorrelation function for the hydrogel sample was then obtained by dividing out the contribution from the reference cell using established procedures.[32] For the case of the CCD detector system, scattered light directly from the sample cell was guided through a lens and pinhole aperture assembly to modulate the speckle field and imaged onto the CCD detector chip of a Dalsa CA-D1−256A camera. Speckle data from the CCD camera was collected by a National Instruments frame-grabber board and analyzed with a single-tau multispeckle correlation program using the Lab Windows package from National Instruments.[31] The resulting composite ensemble-averaged intensity autocorrelation functions obtained from the separate PMT and CCD detection systems were used to calculate the mean square displacement, $\langle \Delta r^2(t) \rangle$, of the fluctuating tracer particles and the local creep compliance $J_m(t)$ using established analysis methods.[33,34]

Mechanical Rheometry. The macroscopic viscoelasticty of the WPT2−3R hydrogels was investigated in a cone and plate geometry using a stress controlled rheometer (Paar Physica MCR300) equipped with a Peltier temperature control device. Samples of pre-made hydrogel were loaded into a 25 mm cone and plate tool and environmentally isolated using a silicone oil vapor barrier. The linear dynamic shear modulus, $G^*(\omega)$, was obtained by operating the rheometer in a controlled strain feed-back mode and performing small amplitude oscillatory strain measurements (1% strain) as a function of frequency and temperature.

Cell Culture. Human foreskin fibroblasts (HFF) obtained from ATCC were routinely grown in RPMI 1640 media containing 300 mg/mL L-glutamine (Gibco), 10% FBS (Gibco), and 100 units/mL of penicillin and 100 μg/mL of streptomycin (Gibco). Cultures were maintained in a humidified incubator at 37 °C and 5% CO_2 and, when nearly confluent, harvested with a solution of 0.25% trypsin in 0.53 mM EDTA (Gibco). For experiments, the cells were re-suspended in serum-free RPMI media before loading onto test surfaces. The test surfaces were coated with variable compositions of the bioactive protein WPT2−3R and its inert counterpart WPT2 by passive adsorption. Unless otherwise specified, protein solutions were prepared at a concentration of 1 mg/mL in pH 7.4 PBS (Gibco), then pipetted onto the test surfaces and incubated for 1 h at room temperature. Prior to seeding the cells, test surfaces were sterilized by UV illumination and rinsed three times with PBS to remove any soluble protein that is not associated with the test surface. Uncoated tissue culture polystyrene (TCPS) was used as a positive control.

Cell Viability. HFF viability on protein coated surfaces was evaluated using the CellTiter 96 AQ_{ueous} One Solution Cell Proliferation Assay (Promega) with a slight modification. In preparation for the assay, 100 μL of cells were loaded into protein coated wells of a 96-well tissue culture plate (BD Falcon) at a density of ~7500 cells/well and cultured for various times between 2 and 12 h to allow for cell adhesion to the substrate. The plate was then removed from the incubator and its liquid contents were gently blotted onto a paper towel. After rinsing twice with RPMI, a mixture of 100 μL of RPMI and 20 μL of the tetrazolium salt 3-(4,5-dimethylthiazol-2-yl)-5-(3-carboxymethoxy-

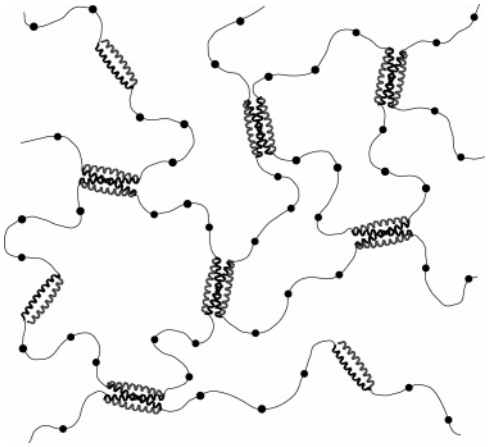

Figure 2. Schematic WPT2−3R hydrogel topology showing dimeric and tetrameric helix bundles of A (gray) and B (black) leucine zipper domains linked by disordered coil domains with three copies of the RGD integrin binding ligand (filled circles).

phenyl)-2-(4-sulfophenyl)-2H-tetrazolium (MTS) was added to each of the wells. The plate was then returned to the incubator for a period of 4 h, after which the absorbance at 490 nm was monitored using an optical plate reader.

Fluorescence Microscopy. Fluorescent staining of fibroblast cytoskeletal components was performed on HFF cells grown on protein-coated glass coverslips (12 mm diameter) in a 24-well tissue culture plate (BD Falcon) as follows. Prior to adding the coverslips, the wells were treated with a 1% solution of bovine serum albumin (BSA, Sigma-Aldrich) in PBS for 1 h in order to block cell attachment to the well surface. Sterile coverslips were then coated with protein solution (WPT2, WPT2−3R, or a mixture of the two) and incubated overnight at 4 °C in wells. After rinsing off unbound protein with PBS, 300 μL of cell suspension (approximately 20 000 cells/well) was seeded onto the coverslips and the plate placed in the 37 °C incubator for a period of 2−12 h. Subsequently, the plates were placed on ice and the wells rinsed once with RPMI. The cells were then fixed sequentially with 3% paraformaldehyde (PFA) in RPMI (10 min) and 3% PFA in PBS (20 min), quenched with 50 mM NH_4Cl in PBS, and permeabilized for 30 min with 1% BSA/0.075% saponin (Sigma-Aldrich) in PBS (solution A). For vinculin staining, cells were incubated for 1 h at room temperature with mouse anti-human vinculin IgG (Sigma-Aldrich, diluted in solution A), rinsed three times with 0.1% BSA/0.075% saponin in PBS (solution B), then incubated for 45 min with Alexa Fluor 546-conjugated goat anti-mouse IgG (Molecular Probes, diluted in solution B). For actin staining, the cells were incubated with Alexa Fluor 488-conjugated phalloidin (Molecular Probes) in solution B for 45 min. Once labeling was completed, the coverslips were rinsed twice with PBS and mounted onto microscope slides with a small drop of Prolong Antifade reagent (Molecular Probes). The samples were viewed with a Zeiss LSM 510 Meta confocal microscope, and digital images of fluorescently labeled adherent cells were recorded at 488 and 546 nm.

Results and Discussion

The design objective for the bioactive protein WPT2−3R was to develop a modular fibrillar protein that self-assembles into a hydrogel and provides an adhesion ligand for the integrin receptors common to many mammalian cell types, as shown schematically in Figure 2. The overall architecture of this protein is the telechelic triblock motif $AC_{10}B$cys of WPT2 developed by Petka et al.[21−23] WPT2 has three distinctive modules: a soluble disordered coil center block C_{10} flanked by two leucine zipper domains, an acidic zipper A with a terminal hexa-histidine tag and a basic zipper B with a terminal cysteine residue.

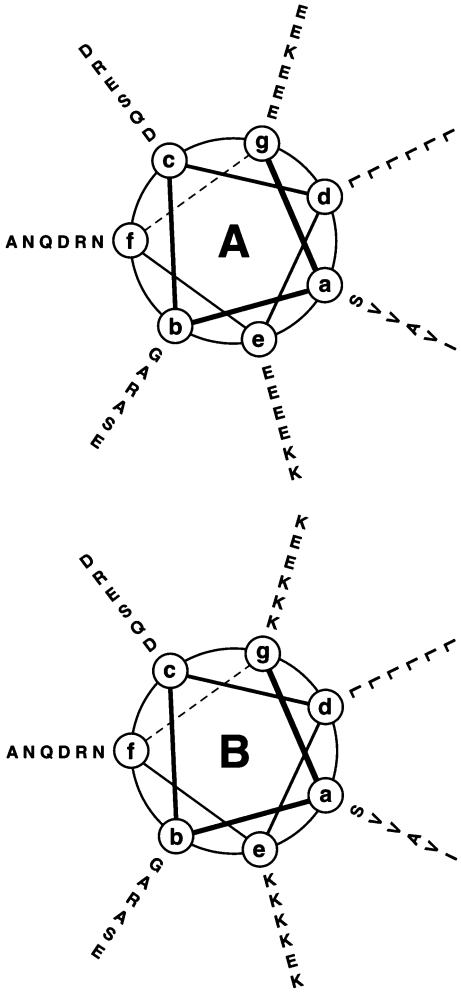

Figure 3. Helix wheel diagrams for the acidic A and basic B leucine zipper.

The leucine zipper is a ubiquitous structural motif in nature characterized by a repetitive heptad pattern, (**abcdefg**), in which **a** and **d** are hydrophobic amino acids (often leucine or isoleucine) and **e** and **g** are charged residues.[35−50] Similar coiled-coil constructs[51−53] have also been successfully utilized for the design of other protein assemblies.[54] In WPT2 and WPT2−3R, the A domains contain primarily glutamic acid residues (E) in the **e** and **g** positions, whereas the B domains have primarily basic lysine residues (K) at **e** and **g**. In moderate temperature and pH conditions, a leucine zipper domain in aqueous solution forms an amphiphilic α-helix with a hydrophobic binding strip composed of the **a** and **d** position residues. Flanking this hydrophobic strip are the charged residues in the **e** and **g** positions, which are partially responsible for the pH-dependent stability of the α-helices. Helix wheel diagrams for the A and B helices are shown in Figure 3.

In solution, the association of these helices into bundles with an internal hydrophobic core region occurs, so as to protect the hydrophobic strips from the polar solution environment. Association into dimers, trimers, or tetramers is commonly observed, although higher order aggregates can form. Interhelical electrostatic interactions, primarily between **e** and **g** positions, modulate the stability of such helical bundles and may lead to pH-dependent association behavior.[47−50] For both WPT2 and WPT2−3R, favorable electrostatic interactions in moderate pH conditions between the acidic residues in the **e** and **g** positions of helix A and the basic residues in the **e** and **g**

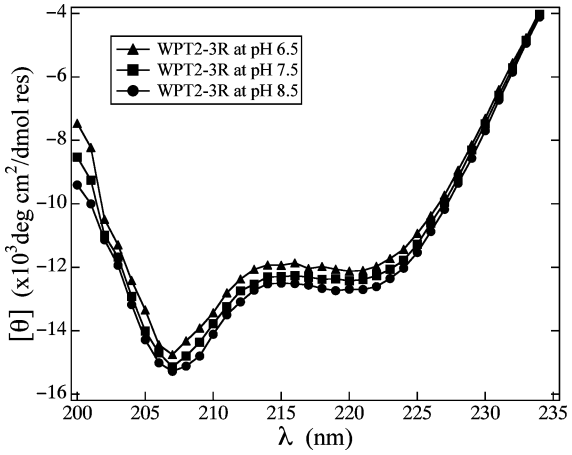

Figure 4. CD wavelength scans for 2.5 μM solutions of WPT2−3R in 10 mM sodium borate phosphate buffer at 25 °C and pH 6.5, 7.5, and 8.5.

positions of helix B are expected to stabilize heteromeric bundles of A and B helices relative to homomeric helix bundles of A or B.

In both WPT2 and WPT2−3R, intermolecular association of A and B helices into bundles induces the formation of a hydrogel network, with the helix bundles serving as cross-links connected by the central disordered coil domains. In the case of WPT2, this central block is composed of 10 repeats of the AGAGAG-PEG sequence, an established disordered coil design that is soluble in aqueous buffers at moderate-to-high pH due to the presence of the glutamic acid residues. In WPT2−3R, the center spacer domain of WPT2 has been modified to include three copies of the RGD integrin binding sequence. As shown below, the presence of the RGD sequences in the center block supports the adhesion of HFF cells without adversely affecting the secondary structure of the A and B end domains or the viscoelasticty of the hydrogels formed by self-assembly of the proteins.

Protein Synthesis. WPT2−3R and WPT2 were synthesized biologically in *E. coli* in a batch-mode fermentor and purified as described above. The amino acid sequences for WPT2 and WPT2−3R are given in Figure 1. WPT2−3R has 251 amino acid residues and a molecular weight of 24 597 Da, whereas the original WPT2 has 230 amino acid residues and a molecular weight of 22 447 Da. The purified target protein yield was typically 100−200 mg per liter of growth media. The purified proteins were analyzed by reverse-phase HPLC, SDS−PAGE, and MALDI-TOF to characterize protein molecular weight and purity. Reverse-phase HPLC analysis showed that the purity of the proteins after Ni−NTA affinity chromatography was at least 96%. MALDI-TOF measurements of WPT2−3R yielded $[M+H]^+$ and $[M+H]^{2+}$ ionization peaks at 24 588 and 12 287, respectively, in good agreement with the calculated molecular weight of 24 597. Together with amino acid analysis, this confirmed the expected sequence of WPT2−3R. Similar agreement between observed and calculated protein sequence was reported for WPT2.[21]

Secondary Structure. To characterize the secondary structure of WPT2−3R in aqueous solution, CD studies were conducted as a function of pH. Figure 4 shows plots of mean residue molar ellipticity [Θ] versus wavelength λ for 2.5 μM solutions of WPT2−3R in 10 mM sodium borate phosphate buffer at 25 °C for three values of pH (6.5, 7.5, and 8.5). The two local minima near 208 and 222 nm are indicative of helical content in the secondary structure of WPT2−3R. As with the triblock constructs developed by Petka et al.,[21−23] the expected secondary structure of WPT2−3R is a combination of helical end domains and a disordered coil center block. The observed form of [Θ], with no apparent local minimum at 218 nm (from potential β-sheet structure) and with a ratio of ellipticities at 222 and 208 nm that is less than unity, is consistent with this expectation. For helix-coil proteins with a large fraction of disordered coil content, which exhibits increasingly negative ellipticity at short wavelengths, the ratio $r = [\Theta]_{222}/[\Theta]_{208}$ may be less than one. The fractional helical content f may be estimated by the ratio of the observed value of [Θ] at $\lambda = 222$ nm to the value for a helical sequence of amino acids as determined from a representative set of proteins with known secondary structure. To facilitate comparison with the previous work on proteins containing the A and B sequences,[21,37] we use the approach of Chen et al.[28] and estimate the fractional helical content as $f = [\Theta]_{222}/[\Theta^{helix}]_{222}$, where $[\Theta^{helix}]_{222} = -39\,500(1 - 2.57/n)$, where n is the number of residues in the protein. The resulting values of r and f corresponding to the CD scans in Figure 4 are given in Table 1.

Table 1. Data and Parameters for WPT2−3R CD Scans at 25 °C

pH	$[\Theta]_{208}$	$[\Theta]_{222}$	r	f
6.5	-14.3×10^3	-12.0×10^3	0.84	0.31
7.5	-14.8×10^3	-12.3×10^3	0.83	0.32
8.5	-15.1×10^3	-12.6×10^3	0.83	0.32

The leucine zipper regions of WPT2−3R are comprised of two sets of six heptad repeats for a total of 84 amino acid residues. Thus, they account for 33% of the entire triblock protein sequence. As determined from $[\Theta]_{222}$, the helical content for this protein varies between approximately 31% and 32%, indicating that the terminal leucine zipper regions of WPT2−3R are well folded in this range of pH conditions. Similar results were reported in previous CD studies of the individual A and B domains [21,55] and the $AC_{10}A$ triblock construct[21,22] at pH 7.4. Interestingly, the helical content of WPT2−3R is rather insensitive to solution pH and temperature (data not shown). This is in contrast to the behavior of the analogous $AC_{10}A$ triblock proteins with acidic leucine zippers on both termini,[21,22] for which the end domains undergo a reversible helix-coil transition with increasing pH or temperature. The insensitivity of WPT2−3R secondary structure to solution conditions may be an indication that association of A and B leucine zipper domains into hetero-oligomeric bundles is the dominant mode of association in WPT2−3R (and also presumably in WPT2, which has identical end domains). Previous CD studies of A, B, and mixtures of A and B have also demonstrated the enhanced stability of the secondary structure in the mixtures relative to solutions of pure A or B.[21,55] We postulate that salt bridges resulting from the complimentary electrostatic interactions between A and B helices in a bundle act to stabilize the secondary structure of individual α-helical leucine zipper domains in solutions of WPT2−3R. In solution, these hetero-oligomeric helix bundles would arise from a combination of inter- and intramolecular association. For the dilute solution conditions utilized in CD measurements, intramolecular association may dominate, leading to the formation of loops. However, at the higher concentrations appropriate for hydrogel formation, intermolecular association is increasingly favorable, and the enhanced stability of hetero-oligomeric helix bundles would translate into enhanced stability of the hydrogel network, as discussed below. It should also be mentioned that intermolecular disulfide bonding generally occurs between the terminal Cys residues, resulting in the formation of linear dimers

of the WPT2−3R triblocks. This dimerization, however, is expected to have minimal impact on hydrogel self-assembly.[21]

Hydrogel Viscoelasticity. Solutions of WPT2 and WPT2−3R both form translucent hydrogel phases at concentrations above approximately 50 mg/mL (5 wt %) in a range of solution pH and temperature conditions. The mechanism for hydrogel formation is presumably the self-assembly of the triblock proteins into a network structure with the intermolecular helix bundles serving as the physical cross-links of the network. The minimal state of oligomerization of these helix bundles required to form a viable network is three, as association exclusively into dimers would only lead to the assembly of long linear chains or cycles of the triblock units. Thus, the observation of hydrogel formation is indirect evidence that the population of helix bundles includes a substantial portion of oligomers larger than dimers. Previous studies of the association behavior of solutions of individual A and B domains indicated the existence of a substantial population of tetramers in equilibrium with dimers,[21,55] suggesting that the active, network-forming cross-links in the hydrogel are primarily tetrameric bundles of the A and B helical domains. As in many telechelic associating polymer systems,[56,57] the self-assembly of these bundles is driven by the hydrophobic effect: the amphiphilic helical members of any given bundle associate in order to protect their hydrophobic faces from direct contact with the aqueous solution. Accordingly, these bundles serve as transient, physical cross-links in the hydrogel, and the helices in a given cross-link bundle may freely exchange with members of nearby bundles, leading to a hydrogel that gradually creeps under an applied load.

We have used DWS microrheology to study the viscoelastic properties of WPT2 and WPT2−3R hydrogels as a function of pH and temperature. In these microrheology studies, the temporal intensity autocorrelation function of light multiply scattered by a dilute suspension of 1 μm diameter tracer particles embedded in the hydrogels was measured and used to monitor the thermally induced fluctuations of the tracer particles.[29,30] The resulting ensemble-averaged mean square tracer particle displacement, $\langle \Delta r^2(t) \rangle$, can be used to obtain microscale rheological response functions for the hydrogels.[33,34] In particular, $\langle \Delta r^2(t) \rangle$ can be used to define a characteristic local creep compliance, $J_m(t) \equiv a\langle \Delta r^2(t) \rangle / k_B T$, where a is the tracer particle radius and $k_B T$ is the terminal energy scale. Microrheology provides unique information about local dynamics and mechanics over a wide range of time scales and is sensitive to molecular relaxation processes. Thus, it is very well suited for monitoring the subtle local creep behavior in these hydrogels. DWS microrheology requires only small volume samples which may be well isolated from their surroundings for extended periods of time by sealing them in optical cuvettes. As data is obtained by optically monitoring thermal fluctuations in well-isolated hydrogels, this is also a relatively noninvasive method to study hydrogel viscoelasticity.

Figure 5 shows plots of $J_m(t)$ obtained at a temperature of 37 °C for 7.5% (w/v) solutions of WPT2−3R in 100 mM sodium borate phosphate buffer at pH 7.5, 8.0, and 9.0. For comparison, the plot also includes $J_m(t)$ for a corresponding pH 7.5 sample of WPT2. In all cases, the $J_m(t)$ exhibit a complex three-stage behavior with a regime of local tracer mobility at early times, a pseudo-plateau region in which tracer particle displacement is restricted at intermediate times, and a final terminal regime of unrestricted tracer particle mobility at late times. The initial regime is associated with the rapid fluctuations of the tracer particles that occur on short length scales in the gels. These fluctuations probe the local dynamics on the molecular scale and may also be sensitive to local rearrangements of the gel microstructure that result from cross-link member exchange processes. The intermediate pseudo-plateau regime reflects the transient elastic response of the gel to sufficiently large tracer particle excursions, and provides a rough measure of the plateau shear modulus, G_p. For a flat plateau, $G_p \sim 1/J_p$, where J_p is a characteristic plateau value of $J_m(t)$. Choosing $J_p = J_m(t = 0.25\ \text{s})$ gives a range of values from $G_p \cong 800$ Pa for WPT2−3R at pH 7.5 to $G_p \cong 1000$ Pa for WPT2−3R at pH 9. For comparison, WPT2 at pH 7.5 has $G_p \cong 650$ Pa, somewhat softer than WPT2−3R in the same conditions.[58] Closer inspection of the data indicates that J_m is not flat in this pseudo-plateau region but exhibits weak power law behavior, $J_m(t) \sim t^{\alpha}$, with α varying from $\alpha \cong 0.03$ (at pH 9) to $\alpha \cong 0.05$ (at pH 7.5). Such behavior is indicative of slow creep behavior, and implies that the local dynamic storage and loss moduli in the pseudo-plateau region scale with frequency as $G'(\omega)_m \sim G''(\omega)_m \sim \omega^{\alpha}$ with $G''_m/G'_m = \pi\alpha/2$. This power-law gel behavior is also observed in macroscopic mechanical rheology measurements on these hydrogels. For instance, Figure 6 shows the dynamic storage and loss moduli, $G'(\omega)$ and $G''(\omega)$, obtained in a small amplitude oscillatory strain measurement of a 7.5% (w/v) solution of WPT2−3R in 100 mM sodium borate phosphate buffer at pH 7.5 and 37 °C. The data show that the

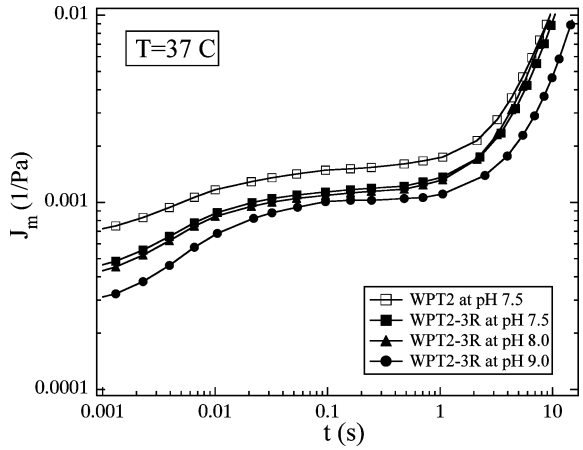

Figure 5. Plots of the local creep compliance $J_m(t)$ at 37 °C for 7.5% (w/v) protein hydrogels in 100 mM sodium borate phosphate buffer with 0.5% (w/v) 1μm latex tracer particles. The filled squares, triangles, and circles correspond to data for WPT2−3R gels at pH 7.5, 8.0, and 9.0, respectively. The open squares correspond to data for a WPT2 gel at pH 7.5

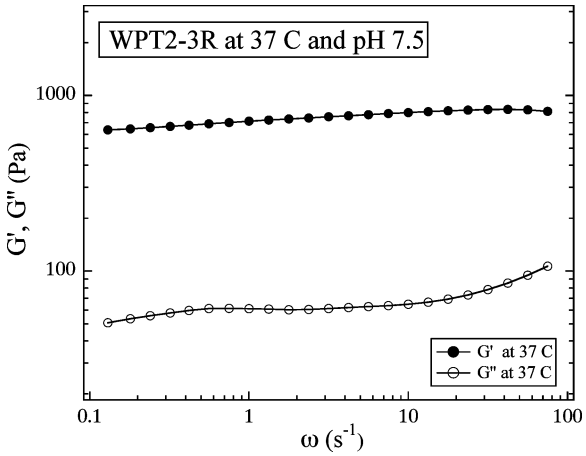

Figure 6. Plots of the dynamic storage and loss moduli, $G'(\omega)$ and $G''(\omega)$, for a 7.5% (w/v) WPT2−3R gel in 100 mM sodium borate phosphate buffer at pH 7.5 and 37 °C.

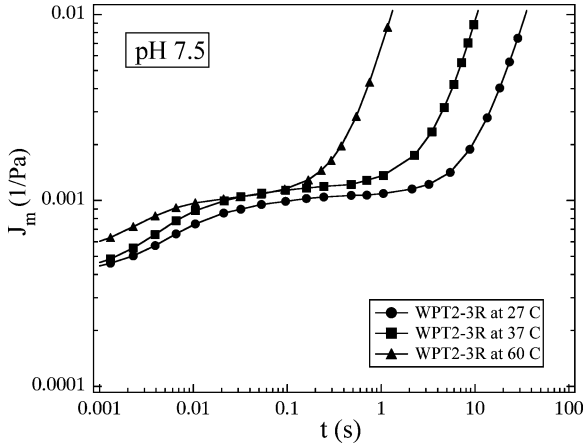

Figure 7. Plots of the local creep compliance $J_m(t)$ at pH 7.5 for 7.5% (w/v) WPT2−3R hydrogels in 100 mM sodium borate phosphate buffer with 0.5% (w/v) 1μm latex tracer particles. The filled circles, squares, and triangles correspond to data for WPT2−3R gels at 27, 37, and 60 °C, respectively.

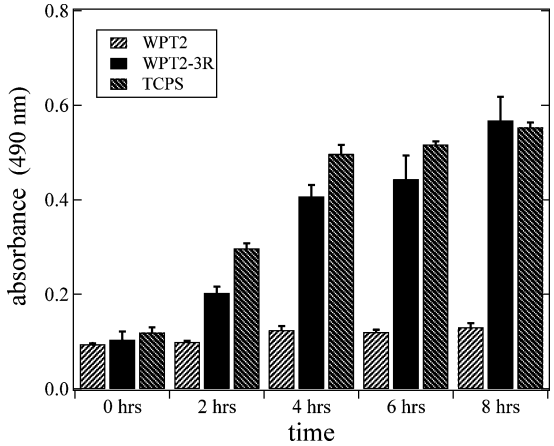

Figure 8. Absorbance at 490 nm as a function of culture time for adherent HFF cells incubated in the presence of MTS. Data are shown for cells on WPT2 and WPT2−3R coated surfaces and for cells on tissue culture polystyrene (TCPS) at 0, 2, 4, 6, and 8 h after initial seeding. Cells were incubated with the MTS reagent for a period of 4 h.

storage modulus exhibits power law behavior, $G'(\omega) \sim \omega^{\alpha}$ with $\alpha \cong 0.05$, over almost three decades of frequencies.[59] Although the loss modulus does not follow such a clear power law form, the magnitude of the storage modulus, $G' \cong 770$ Pa, and the ratio of the loss and storage moduli, $G''/G' \cong 0.08$, at $\omega = 4.2$ s^{-1} are consistent with the values inferred from the microrheology measurements, namely $G_p \cong 800$ Pa and $G''/G' \cong 0.078$.

The terminal relaxation behavior of WPT2 and WPT2−3R is similar to that observed in many self-associating polymer systems. For the 37 °C data shown in Figure 5, the terminal relaxation times of these proteins are very similar, varying from $\tau_r \cong 18$ s for WPT2 and WPT2−3R at pH 7.5 to $\tau_r \cong 25.5$ s for WPT2−3R at pH 9. The similarity of τ_r for WPT2 and WPT2−3R is expected since the characteristic relaxation time in telechelic systems is determined primarily by the lifetime of the associating end domains, which are identical for the two proteins. The terminal relaxation time is, however, sensitive to temperature. Figure 7 shows plots of $J_m(t)$ obtained for 7.5% (w/v) solutions of WPT2−3R in 100 mM sodium borate phosphate buffer at pH 7.5 and temperatures of 27, 37, and 60 °C. Increasing the temperature reduces τ_r, which scales as $\tau_r(T) \sim \exp(\Delta G/RT)$ consistent with the characteristic activated terminal relaxation observed in many associating polymer systems.[57] The apparent activation energy of $\Delta G \cong 80$ kJ/mol corresponds to approximately 30 k_BT per cross-link, assuming that each end domain is a member of an active cross-link bundle. This estimate, while very crude, is reasonable for the leucine zipper end domains, which have 12 nonpolar residues per hydrophobic face.

Protein−Fibroblast Interactions. The RGD tripeptide sequence embedded in the central spacer block of WPT2−3R is a known ligand for integrin receptors displayed on the surface of many mammalian cell lines. The efficacy of RGD binding to cell surface integrins depends on the density of ligands in the RGD-containing hydrogel and on the presentation of the ligand to the integrin receptor. The former is controlled by the hydrogel architecture and can be modulated by forming mixed hydrogels of biofucntional WPT2−3R proteins with bioinert WPT2 proteins. The latter depends on the conformation of the spacer block in the vicinity of the ligand sequence. The disordered coil spacer block in WPT2−3R is expected to provide favorable conditions for the display of embedded ligands. Effective presentation of RGD ligands in turn facilitates adhesion of cells to the hydrogel and the subsequent formation of focal adhesion complexes, the hallmark of integrin activation in cells. The response of human foreskin fibroblasts (HFF) to both WPT2 and WPT2−3R gels was characterized in cell culture experiments on protein-coated surfaces. Both cell viability and cytoskeletal fluorescence assays were performed. The viability assay monitors metabolic activity in adherent cells through the reduction of MTS tetrazolium salt by dehydrogenases to formazan, which is detected colorimetrically by absorbance at 490 nm in an optical plate reader. Figure 8 shows absorbance at 490 nm as a function of incubation time for HFF cells seeded onto WPT2 and WPT2−3R coated wells of a 96-well tissue culture plate. The response is indicated at 0, 2, 4, 6, and 8 h after initially seeding the cells. The data shown in the figure is the result of averaging over 3 equivalent wells for each protein. As a positive control, the response of cells to bare tissue culture polystyrene (TCPS) wells is also shown. The data in the figure shows that the biofunctional WPT2−3R coated wells elicit similar response to the TCPS wells after about 6 h of culture. In contrast, the bio-inert WPT2 coated wells show a low level of response for the duration of the cell culture period, indicating that the WPT2 inhibits cell viability on coated surfaces. For both WPT2 and WPT2−3R surfaces, there seemed to be little or no qualitative changes in cell response after 8 h of culture in serum free media.[60]

Inspection of cell-seeded WPT2 and WPT2−3R coated surfaces by optical microscopy indicated that far fewer adherent cells are found on WPT2 surfaces than on the WPT2−3R surfaces. Moreover, those cells observed on WPT2 surfaces generally did not spread but maintained a rounded morphology. In contrast, cells observed on WPT2−3R surfaces exhibited the phenotypical well-spread and polarized morphology[61] expected for adherent fibroblasts. More detailed information about the response of HFFs to these protein coated surfaces was obtained from confocal microscopy studies. In these studies, HFF cells cultured on WPT2 and WPT2−3R coated glass surfaces were fixed and permeablized, and fluorescent staining of the fibroblast cytoskeletal proteins actin and vinculin, a protein associated with focal adhesions, was performed. For actin staining, the cells were incubated with Alexa Fluor 488-conjugated phalloidin. For vinculin staining, cells were incubated with mouse anti-human vinculin IgG followed by incubation with Alexa Fluor 546-conjugated goat anti-mouse IgG, as described in the methods

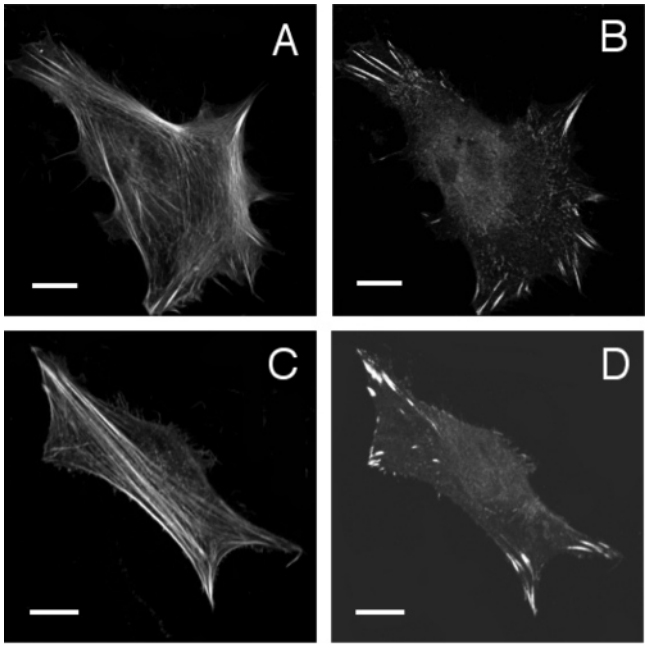

Figure 9. Confocal microscopy images of two representative HFF cells cultured on WPT2−3R coated glass surfaces. Images A and C show fluorescently labeled actin in each cell, whereas images B and D show fluorescently labeled vinculin. White scale bars are 20 microns in length.

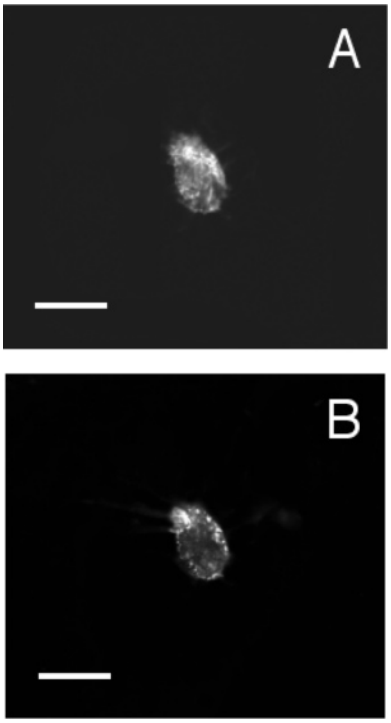

Figure 10. Confocal microscopy images of a HFF cell cultured on a WPT2 coated glass surface. Image A shows fluorescently labeled actin, while image B shows fluorescently labeled vinculin. White scale bars are 20 microns in length.

section. Figure 9 shows confocal microscopy images of two representative HFF cells cultured on WPT2−3R coated glass surfaces for 6 h. In Figure 9, panels A and C, fluorescently labeled actin is shown in each cell, whereas in Figure 9, panels B and D, the corresponding fluorescently labeled vinculin is shown. Both cells clearly exhibit the characteristic polarized morphology[61] of adherent fibroblasts with well-developed actin stress fibers terminating at focal adhesions. This response is evident within 2 h of initial cell seeding onto WPT2−3R surfaces (data not shown). In contrast, cell polarization and the development of an actin stress fiber network does not occur in cells cultured on WPT2 coated surfaces. Figure 10 shows confocal microscopy images of a representative HFF cell cultured on a bioneutral WPT2 surface for 6 h. Fluorescently labeled actin and vinculin are shown in Figure 10, panels A and B, respectively. In this case, the cell has a rounded morphology indicative of a poorly adherent cell and lacks organized actin stress fibers (see Figure 10A) and well-defined focal adhesions (see Figure 10B). This response is independent of cell culture duration, suggesting that WPT2 surfaces not only lack the biochemical signals for integrin activation and focal adhesion formation but also inhibit adsorption of natural ECM proteins secreted by the cells or otherwise present in the media.

Since the associating domains are identical in WPT2 and WPT2−3R, mixed hydrogels may be formed from these two proteins. In this way, the number density of the bioactive RGD ligands may be continuously varied from zero in WPT2 to the maximum value for pure WPT2−3R. Since cell-substratum interaction is dependent on the surface density of the minimal integrin-binding peptides, the utility of the bioactive-bioinert mixtures is the potential to modulate cell adhesion and response by varying the density of RGD ligands in the biomaterial. Confocal microscopy studies performed for HFF cells on mixed WPT2/WPT2−3R coated surfaces support this idea. We found that spread and polarized fibroblasts with fully developed focal adhesion complexes occur within 6 h of culture on mixed hydrogels with as little as 10% WPT2−3R (data not shown). Moreover, the relative fraction of adherent cells and the apparent spreading area of adherent cells increases with the fraction of bioactive WPT2−3R protein in a mixed layer.[27]

Conclusions

Hydrogels with integrin binding activity were created from associating proteins with embedded RGD sequences. These proteins are modified AC_{10}Bcys triblock designs[21,22] composed of acidic and basic leucine zipper associating domains flanking a soluble disordered coil block that contains three copies of the RGD tripeptide sequence.[62] The synthetic gene encoding this modified central block was also re-designed to remove repetition at the DNA codon level, to facilitate insertion and modification of bioactive domains.[24,27] The secondary structure of the proteins and the mechanical properties of the hydrogels they form were not adversely affected by the presence of the RGD sequences. In fact, the plateau elastic modulus extracted from microrheology measurements was slightly higher for the RGD containing proteins (WPT2−3R) than the original AC_{10}Bcys design (WPT2), possibly due to increased center block solubility.[58] The inclusion of the RGD sequences in the disordered coil region was shown to support the adhesion, spreading, and polarization of human fibroblast cells on WPT2−3R protein coated surfaces.[62] In particular, confocal microscopy studies demonstrated the presence of focal adhesion complexes and organized actin stress fibers in these cells. In contrast, fibroblasts seeded onto surfaces coated with WPT2 remained rounded and did not form focal adhesions.

These associating proteins are a class of telechelic polymers that form regular, self-assembling hydrogel networks by physical association of end domains. The fact that physical association of the end domains is highly regulated, forming predominantly tetrameric cross-links with some dimeric ones, is the source of the structural regularity of these materials and is one of the clear

advantages of this approach to hydrogel materials. Another advantage is the modular design of their protein components. The physical properties of these hydrogel materials depend on the attributes of both the soluble center domain and the associating end domains, while the biological functionality is encoded into the center block. For instance, the mechanical properties of the hydrogels are determined by the composition and stability of the leucine zipper assemblies and by the solubility and length of the center domain. As the center and end domains may be independently engineered, the structural and mechanical properties of these modular protein hydrogels may be tailored to suit particular applications. The current design forms robust space-filling networks at concentrations above approximately 5 wt % (50 mg/mL) with plateau values of the shear elastic modulus in the range of 10^2-10^3 Pa. This is slightly higher than many synthetic and biological hydrogels of this modulus, which typically are composed of a few weight percent of macromolecules but which are usually more heterogeneous in structure. One may easily lower the threshold value of gelation in these proteins by increasing the length of the spacer block, at the cost of reduced modulus. Alternatively, one may increase the modulus simply by shortening the center block.

This approach to biofunctional materials has potential for cell and tissue culture applications. As alternatives to RGD, a number of different cell binding polypeptide sequences may easily be incorporated into the center block, allowing for the creation of a library of biofunctional proteins. These proteins, either individually or in combinations, would self-assemble into hydrogels with ligands for various cell surface receptors. This ability to easily modify the biofunctional attributes of these systems is another advantage of protein-based hydrogel materials for biomedical applications. One potential drawback to the use of these proteins is their stability in biological environments. As they form hydrogels by reversible self-assembly, these gels will slowly dissolve when placed in contact with excess cell culture media. However, once assembled such hydrogels could be chemically cross-linked using standard commercial reagents for amine chemistry, if necessary, to inhibit dissolution. Moreover, since the associating end domains strongly adsorb to many polymeric and inorganic surfaces, these proteins would also be useful for functionalizing surfaces. A library of such proteins could also be utilized to assemble combinatorial cell binding arrays for use in fundamental studies of cell-biomaterials interactions, for instance. As for cell and tissue engineering applications, porous cell scaffold materials such as polymer foams could be coated with selected biofunctional proteins and thereby acquire the ability to interact biochemically with specific cell surface receptors. This would provide a simple route to tailoring otherwise bioinert surfaces for particular cell and tissue culture applications. We note that in such cell and tissue engineering applications, the purpose of these biofunctional protein materials is primarily a transient one: to guide the adhesion of cells to the scaffold and to provide biochemical cues to initiate desired cell response. Having set up the initial conditions for cell and tissue culture, these proteins are expected to be degraded by cell-secreted proteases and removed from the system, allowing natural cell-secreted ECM constituents to take their place.

Acknowledgment. This work was supported by NASA through grant NAG 9-1345. We thank David Tirrell for discussions and for generously providing the expression plasmid pQE9-L2AC_{10}B for the original triblock protein AC_{10}Bcys. We also thank Chong Lee, Wendy Petka, and Jill Sakata for assistance in the early stages of this work, and the Integrated Imaging Center at JHU for use of confocal microscopy facilities.

References and Notes

(1) Hubbell, J. A *Curr. Opin. Biotechnol.* **1999**, *10*, 123−129.
(2) *Protein-Based Materials*; McGrath, K., Kaplan, D., Eds.; Birkhauser: Boston, 1999.
(3) Yamada, K. M. *J. Biol. Chem.* **1991**, *266*, 12809−12812.
(4) Ruoslahti, E. *Annu. Rev. Cell Dev. Biol.* **1996**, *12*, 697−715.
(5) Buck, C. A.; Horwitz, A. F. *Annu. Rev. Cell Biol.* **1987**, *3*, 179−205.
(6) Horn D. L.; Hubbell J. A. *J Biomed. Mater. Res.* **1998**, *39*, 266−276.
(7) Bearinger, J. P.; Castner, D. G.; Healy, K. E. *J. Biomater. Sci. Polym. Ed.* **1998**, *9*, 629−652.
(8) Rowley, J. A.; Madlambayan, G.; Mooney, D. J. *Biomaterials* **1999**, *20*, 45−53.
(9) Schense, J. C.; Hubbell, J. A. *J. Biol. Chem.* **2000**, *275*, 6813−6818.
(10) Park, Y. D.; Tirelli, N.; Hubbell, J. A. *Biomaterials* **2003**, *24*, 893−900.
(11) Cook, A. D.; Hrkach, J. S.; Gao, N. N.; Johnson, I. M.; Pajvani, U. B.; Cannizzaro, S. M.; Langer, R. *J. Biomed. Mater. Res.* **1997**, *35*, 513−523.
(12) Wang, D. A.; Ji, J.; Sun, Y. H.; Shen, J. C.; Feng, L. X.; Elisseeff, J. H. *Biomacromolecules* **2002**, *3*, 1286−1295.
(13) Dillow, A. K.; Ochsenhirt, S. E.; McCarthy, J. B.; Fields, G. B.; Tirrell, M. *Biomaterials* **2001**, *22*, 1493−1505.
(14) Sofia, S.; McCarthy, M. B.; Gronowicz, G.; Kaplan, D. L. *J. Biomed. Mater. Res.* **2001**, *54*, 139−148.
(15) Chen, J. S.; Altman, G. H.; Karageorgiou, V.; Horan, R.; Collette, A.; Volloch, V.; Colabro, T.; Kaplan, D. L. *J. Biomed. Mater. Res. A* **2003**, *67A*, 559−570.
(16) Urry, D. W.; Pattanaik, A.; Xu, J.; Woods, T. C.; McPherson, D. T.; Parker, T. M. *J. Biomater. Sci. Polym. Ed.* **1998**, *9*, 1015−1048.
(17) Kobatake, E.; Onoda, K.; Yanagida, Y.; Haruyama, T.; Aizawa, M. *Biotechnol. Tech.* **1999**, *13*, 23−27.
(18) Panitch, A.; Yamaoka, T.; Fournier, M. J.; Mason, T. L.; Tirrell, D. A. *Macromolecules* **1999**, *32*, 1701−1703.
(19) Heilshorn, S. C.; DiZio, K. A.; Welsh, E. R.; Tirrell, D. A. *Biomaterials* **2003**, *24*, 4245−4252.
(20) Liu, J. C.; Heilshorn, S. C.; Tirrell, D. A. *Biomacromolecules* **2004**, *5*, 497−504.
(21) Petka, W. A. Reversible gelation of genetically engineered macxomolecules. Ph.D. Thesis, University of Massachusetts, Amherst, 1997.
(22) Petka, W. A.; Harden, J. L.; McGrath, K. P.; Wirtz, D.; Tirrell, D. A. *Science* **1998**, *281*, 389−392.
(23) Petka, W. A.; Harden, J. L.; Sakata, J. K.; Tirrell, D. A. *Mater. Res. Soc. Symp. Proc.* **1999**, *550*, 23−28.
(24) Mi, L.; Harden, J. L. *Biomacromolecules* **2006**, submitted.
(25) *Short Protocols in Molecular Biology*, 5th ed.; Ausubel, F. M., et al. Eds.; John Wiley & Sons: New York, 2002.
(26) *Molecular cloning: a laboratory manual*, 3rd ed.; Sambrook, J., Russell, D. W., Sambrook, J., Eds.; Cold Spring Harbor Laboratory: Cold Spring Harbor, New York, 2001.
(27) Mi, L. Protein hydrogels with engineered biomolecular recognition. Ph.D. Thesis, Johns Hopkins University, Baltimore, MD, 2003.
(28) Chen, Y. H.; Yang, J. T.; Chau, K. H. *Biochemistry* **1974**, *13*, 3350−3359.
(29) Weitz, D. A.; Pine, D. J. Diffusing Wave Spectroscopy. In *Dynamic Light Scattering; The Method and Some Applications*; Brown, W., Ed.; Clarendon: Oxford, U.K., 1993; p 719.
(30) Harden, J. L.; Viasnoff, V. *Curr. Opin. Colloid Interface Sci.* **2001**, *6*, 438−445.
(31) Viasnoff, V.; Lequeux, F.; Pine, D. J. *Rev. Sci. Instrum.* **2002**, *73*, 2336−2344.
(32) Scheffold, F.; Skipetrov, S. E.; Romer, S.; Schurtenburger, P. *Phys. Rev. E*, **2001**, *63*, 061404.
(33) Mason, T. G.; Gang, H.; Weitz, D. A. *J. Mol. Struct.* **1996**, *383*, 81−90.
(34) Mason, T. G. *Rheol. Acta* **2000**, *39*, 371−378.
(35) Hodges, R. S.; Saund, A. K.; Chong, P. C. S.; St.-Pierre, S. A.; Reid, R. E. *J. Biol. Chem.* **1981**, *256*, 1214−1224.
(36) Lau, S. Y. M.; Taneja, A. K.; Hodges, R. S. *J. Biol. Chem.* **1984** *259*, 3253−3261.
(37) Landschulz, W. H.; Johnson, P. F.; McKnight, S. L. *Science* **1988**, *240*, 1759−1764.

(38) DeGrado, W. F.; Wasserman, Z. R.; Lear, J. D. *Science* **1989**, *243*, 622−628.
(39) O'Shea, E. K.; Rutkowski, R.; Stafford, W. F. III; Kim, P. S. *Science* **1989**, *245*, 646−648.
(40) Lupas, A.; Dyke, M. V.; Stock, J. *Science* **1991**, *252*, 1162−1164.
(41) Harbury, P. B.; Zhang, T.; Kim, P. S.; Alber, T. *Science* **1993**, *262*, 1401−1407.
(42) Graddis, T. J.; Myszka, D. G.; Chaiken, I. M. *Biochemistry* **1993**, *32*, 12664−12671.
(43) Monera, O. D.; Zhou, N. E.; Kay, C. M.; Hodges, R. S. *J. Biol. Chem.* **1993**, *268*, 19218−19227.
(44) Harbury, P. B.; Kim, P. S.; Alber, T. *Nature* **1994**, *371*, 80−83.
(45) Lumb, K. J.; Kim, P. S. *Science* **1995**, *268*, 436−439.
(46) Monera, O. D.; Zhou, N. E.; Lavigne, P.; Kay, C. M.; Hodges, R. S. *J. Biol. Chem.* **1996**, *271*, 3995−4001.
(47) Lupas, A. *Trends Biochem. Sci.* **1996**, *21*, 375−382.
(48) Kohn, W. D.; Hodges, R. S. *Trends Biotechnol.* **1998**, *16*, 379−389.
(49) Burkhard, P.; Stetefeld, J.; Strelkov, S. V. *Trends Cell Biol.* **2001**, *11*, 82−88.
(50) Yu, Y. B. *Adv. Drug Delivery Rev.* **2002**, *54*, 1113−1129.
(51) Pandya, M. J.; Spooner, G. M.; Sunde, M.; Thorpe, J. R.; Rodger, A.; Woolfson, D. N. *Biochemistry* **2000**, *39*, 8728−8734.
(52) Zhou, M.; Bentley, D.; Ghosh, I. *J. Am. Chem. Soc.* **2004**, *126*, 734−735.
(53) Potekhin, S. A.; Melnik, T. N.; Popov, V.; Lanina, N. F.; Vazina, A. A.; Rigler, P.; Verdini, A. S.; Corridin, G.; Kajava, A. V. *Chem. Biol.* **2001**, *8*, 1025−1032.
(54) Rajagopal, K.; Schneider, J. P. *Curr. Opin. Struct. Biol.* **2004**, 14, 480−486.
(55) McGrath, K. P.; Butlere, M. M.; DiGirolamo, C. M.; Kaplan, D. L.; Petka, W. P.; Laue, T. M. *J. Bioactive Compatible Polym.* **2000**, *15*, 334−356.
(56) Winnik, M. A.; Yekta, A. *Curr. Opin. Colloid Interface Sci.* **1997**, *2*, 424−436.
(57) Larson, R. G. *The structure and rheology of complex fluids*; Oxford University Press: New York, 1999; Chapter 5.
(58) The solubility of the central block of WPT2−3R may be enhanced with respect to WPT2 due to the additional polar residues included in the design.
(59) It should be noted that traditional mechanical rheometry measurements are less sensitive to local relaxation processes than microrheology techniques. As a result, terminal relaxation times measured in mechanical rheometry tend to be larger than those obtained by microrheometry.
(60) We note that culture in serum-free media presents a serious challenge to the cells for sufficiently long periods.
(61) By polarization, we mean cell elongation associated with an asymmetric cytoskeletal structure.
(62) Three RGD sequences were included in the spacer coil in order to maximize the probability of favorable presentation of the ligand to the cell surface integrin receptors. However, we have found that a single RGD sequence is sufficient in many cases to induce HFF adhesion and spreading.

BM050157P